energies

MDPI

Article

Control of Heat Pumps with CO_2 Emission Intensity Forecasts

Kenneth Leerbeck [1,*], Peder Bacher [1], Rune Grønborg Junker [1], Anna Tveit [1] and Olivier Corradi [2], Henrik Madsen [1,3] and Razgar Ebrahimy [1]

1 Department of Applied Mathematics and Computer Science, Technical University of Denmark, 2800 Lyngby, Denmark; pbac@dtu.dk (P.B); rung@dtu.dk (R.G.J); annatveit@hotmail.com (A.T); hmad@dtu.dk (H.M); raze@dtu.dk (R.E.)

2 Tomorrow (Tmrow IVS), Njalsgade, 2300 Copenhagen, Denmark; olivier.corradi@tmrow.com

3 Faculty of Architecture and Design, Norwegian University of Science and Technology, NO-7491 Trondheim, Norway

* Correspondence: kenle@dtu.dk; Tel.: +45-61427386

Received: 29 April 2020; Accepted: 26 May 2020; Published: 3 June 2020

Abstract: An optimized heat pump control for building heating was developed for minimizing CO_2 emissions from related electrical power generation. The control is using weather and CO_2 emission forecasts as inputs to a Model Predictive Control (MPC)—a multivariate control algorithm using a dynamic process model, constraints and a cost function to be minimized. In a simulation study, the control was applied using weather and power grid conditions during a full-year period in 2017–2018 for the power bidding zone DK2 (East, Denmark). Two scenarios were studied; one with a family house and one with an office building. The buildings were dimensioned based on standards and building codes/regulations. The main results are measured as the CO_2 emission savings relative to a classical thermostatic control. Note that this only measures the gain achieved using the MPC control, that is, the energy flexibility, not the absolute savings. The results show that around 16% of savings could have been achieved during the period in well-insulated new buildings with floor heating. Further, a sensitivity analysis was carried out to evaluate the effect of various building properties, for example, level of insulation and thermal capacity. Danish building codes from 1977 and forward were used as benchmarks for insulation levels. It was shown that both insulation and thermal mass influence the achievable flexibility savings, especially for floor heating. Buildings that comply with building codes later than 1979 could provide flexibility emission savings of around 10%, while buildings that comply with earlier codes provided savings in the range of 0–5% depending on the heating system and thermal mass.

Keywords: heat pumps; model predictive control (MPC); buildings; dynamic systems; CO_2-emissions; electrical grid power

1. Introduction

Energy flexibility on the electricity market is a high focus area in modern energy policies scoping in on storage (e.g., batteries, fuel cells, hydro reservoirs, thermal) and flexible demand (e.g., heat pumps, electric cars) [1]. The aim is to decrease CO_2 emissions by meeting the fluctuating proportion of renewable sources (e.g., solar, wind) vs nonrenewable sources (e.g., coal, gas, nuclear). Ideally, in the future, electricity users (the demand) will respond to the renewable power generation levels in an attempt to minimize emissions—in a 100% renewable scenario storage and flexibility is a must for operating the power system [2].

Therefore, methods for identifying the flexibility potential in various applications are developed. In Reference [3], the energy flexibility potential in buildings is identified by the so-called *Flexibility*

Index, which is the energy cost, from a penalty-aware control, relative to a penalty-ignorant control. The penalty could be for example, a CO_2 or price signal. The present paper investigates the energy flexibility potential in buildings with a focus on heat pumps.

Heat pumps have different sizes and applications, from small single building heat pumps to large heat pumps for district heating. The scope of the present study is limited to investigate the increasing potential in single building heat pumps—which has been almost four-fold from 2011 to 2019 while the number of oil-fired boilers have decreased by roughly one third in the same period [4]. Many oil-fired boilers are replaced with heat pumps—due to both economic and environmental benefits and political pressure (bans of oil-fired boilers in certain districts for new buildings [5].) The control of the heating, however, are often simple thermostatic controls. This often results in heating when electricity demand is high (e.g., afternoon and evening peaks), leading to increased system stress, resulting in increased fossil fuel consumption. It is, therefore, an opportunity to shift the demand away from peak hours using the heat-storing potential of the buildings.

In a power system, the generator which is responding to small changes in demand (e.g., start-up of a heat pump) is called the marginal generator. A reasonable estimate of the marginal generator is achieved by using price signals, see Figure 1—the merit order illustrated with a supply/demand curve; the *x*-axis has the accumulated supply generators and the y-axis is the corresponding price. A small increase in demand (dashed blue line) illustrates the marginal generator—in this case, a coal fired Combined Heat and Power (CHP) plant.

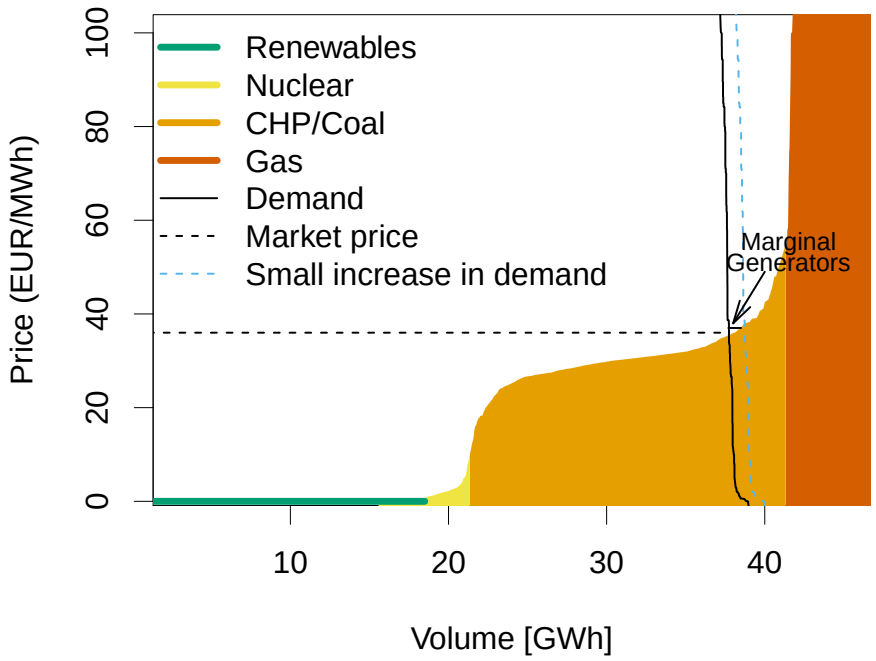

Figure 1. The figure is the merit order illustrated with a supply and demand curve. The *x*-axis is the accumulated generators in the power system and the *y*-axis is their corresponding costs. The highest generator in the merit order is the one crossing with the demand curve—a coal Combined Heat and Power (CHP) plant in this example. The average emissions are a weighted average from all activated generators. The **marginal generator** is the generator that will be activated by moving the demand line slightly to the right (dashed blue line). Data source: Nord Pool AS.

Due to both grid stability, economic and environmental benefits, day-ahead spot price-based control strategies have been proposed in recent papers [6–8], using occupancy mode detection and rule-based price control and Model Predictive Control (MPC) (a multivariate predictive control algorithm using a dynamic process model, constraints and a cost function to be minimized). In Reference [6], MPC is used with varying electricity prices to minimize the cost of operating a heat

pump connected to a storage unit and a floor heating system. The control only heats at night, where the prices are low, and it is assumed that the heat pump and storage are large enough to accumulate enough heat for the whole day. Cost savings of between 25% to 30% are obtained. MPC is a well-known concept in building automation control literature [9–13], and proven to be promising with respect to minimizing costs, but a broad practical implementation still has various challenges discussed in Reference [14].

In Reference [10], the importance of occupancy information is highlighted and evaluated on a daily basis. However, a higher resolution is needed to incorporate variations throughout the day (e.g., when people are at work). In the study in Reference [7] occupancy modes are used together with price signals to control a heat pump. The occupancy modes were developed in The Olympic Peninsula project [15] and describe *work, night* and *home* mode, each with a corresponding set point and price sensitivity. The study showed a significant level of load shifting, leveling out the normal peaks in the daily demand curve. A self-learning controller was applied and adapts easily to changing consumer habits.

There is a problem with spot prices though, known as the merit order emission dilemma, as illustrated in Reference [16] for the German-Austrian power market: The price for coal is low but the emissions are high. A price-based control, therefore, only leads to a decrease in emissions if there is a surplus of renewable energy (more renewable energy than needed)—otherwise coal is favored, and it is therefore encouraged to use CO_2 emission signals instead.

For CO_2 emissions, two distinct measures are used: average and marginal emission intensities, both with the units $\left(\frac{\text{kg}CO_2\text{-eq}}{\text{MWh}}\right)$. Average emissions correspond to the overall, for example, region-wide, electricity production including net imports. The marginal reflects the emissions of the marginal generator. The concepts are compared in Reference [17] and the importance of distinguishing between the two is highlighted due to their very opposing patterns. It is emphasized that the marginal emission is the most optimal signal to use for control.

In Reference [8], the average CO_2 emission intensity and price signals are used in heat pump control of residential buildings in Norway (known for low emissions due to large amount of hydropower) with Predictive Rule-Based Control (uses predefined thresholds to give information about when the emissions are low). it is concluded that with price-based control, the overall CO_2 emissions have actually increased (evaluated using the average emissions). It is argued to result from the load being shifted to the night time, where cheap carbon-intensive electricity is imported from the continental European power grid. This is either a great example of the merit order dilemma or a result that may have been different if marginal emissions had been used.

A recent study [18] investigated marginal emissions and uses estimates provided by Tomorrow (www.tmrow.com) to develop a 24-hour forecast using a machine learning approach on historical data. The CO_2 estimates are calculated with the empirical method developed in Reference [19] using historical data from European bidding zones. The chain of imports (the so-called flow tracing, originally introduced in Reference [20,21]) is followed to assess the impact of a specific generator or load on the power system. This is a large scale solution using data from the majority of bidding zones around the world.

In the present study, MPC is used for control for heating a building. This allows using knowledge of future indoor climate states, CO_2 emissions and weather conditions to schedule heat pump operation. It is a linear approach, which has its limits and requires simplifications, investigated and discussed in Reference [22]. The simplifications include neglecting the effect on the efficiency from factors, for example, frequency variations in the compressor (a main component in a heat pump) and temperature variations. The paper concludes that neglecting these factors can lead to significant errors. The frequency variations are, however, are not used in this study. From Reference [22], the frequency is noticed to be the least important factor and is specifically justified when using varying electricity prices, because the heat pump mostly operates at nominal speed to maximize the heat output when prices are low. The impact from the outdoor temperature is accounted for—this is important because it means the efficiency is lower during the night, where also the emissions are low.

In order to model the heat dynamics in the building, a lumped dynamic process model is applied [23]. A tricky part is to determine the values of the parameters appropriately, for example, insulation level and heat capacity: if the right type of measured data is available, the parameters can be estimated [24], or they can be calculated according to physics. In the present study physics are used and a sensitivity analysis is carried out to map the impact of parameters on the CO_2 savings potential. Such a sensitivity analysis is lacking in the literature. In some papers transparency is lost, since the impact of the parameters is not elucidated, thus increasing the risk of biased results. This paper addresses both of these issues by using historic danish building codes from 1977 and later to describe the insulation thickness as a parameter along with the heat pump size and thermal capacity of floor in two hypothetical buildings: a family house and an office building. Further, the impact of using forecasts is assessed by comparing the savings achieved with known future weather (perfect forecasts) vs. real forecasts.

It is noted that the emission saving potential using an MPC, that is, flexible demand, is measured as CO_2 emission savings relative to classical thermostatic control, that is, non-flexible demand. Hence, the results express only the potential of energy flexibility, not the absolute emission savings.

In Section 2, the weather data and marginal CO_2 emissions are presented. The dynamic process model is presented in Section 3 as an RC-diagram together with the MPC which is written up as a linear programming formulation. The efficiency of the heat pump is modelled as a temperature-dependent variable but neglects the compressor frequency. In Section 4 the building codes, temperature settings and model parameters are discussed. The results are presented in Section 5 as graphs showing the CO_2 emission reductions vs selected parameters—for example, heat pump size, concrete and building regulation year.

2. Data

Data provided by Tomorrow (www.tmrow.com) is used in the study. It comprises the marginal CO_2 emission data and weather forecasts (temperature and solar irradiation) to model the building thermodynamics and heat pump planning—see Figure 2. The emissions show close to none seasonality except the winter, where the intensity peaks. Both the temperature and solar radiation are highly seasonal with a hot climate and high solar radiation in the summer—reversed in the winter.

Only the CO_2 emissions are provided in both real-time values and forecasts. The real-time weather conditions are, however, also essential for the model to describe the actual building thermodynamics. The solar irradiation forecast is plotted in Figure 3 (left plot) for the 21st of June. Every sixth hour a new forecast is provided, at 2 a.m., 8 a.m., 2 p.m. and 8 p.m. The gaps between the forecasts are significant and illustrate the inaccuracy of the prediction for long horizons.

For modelling purposes, the real-time weather conditions are modelled from the forecasts. Assuming horizons for $h = 1$ are the most accurate forecasts, a kernel smoothing process using splines and a weight for short horizon favouritism is applied—see Appendix A for a description of the approach. The result for solar radiation is the smoothing curve seen in Figure 3, right plot. The temperature forecasts did not show any significant gaps, suggesting all horizons, 1–6, are more correct models of the real-time condition than the solar radiation.

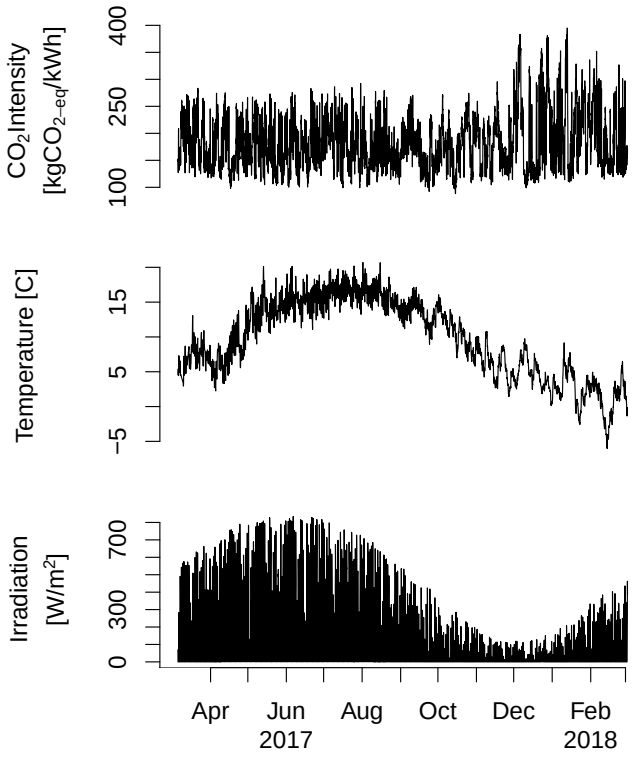

Figure 2. Marginal CO_2 emissions (real-time), Temperature and solar irradiation (forecasts) plotted for the evaluated period.

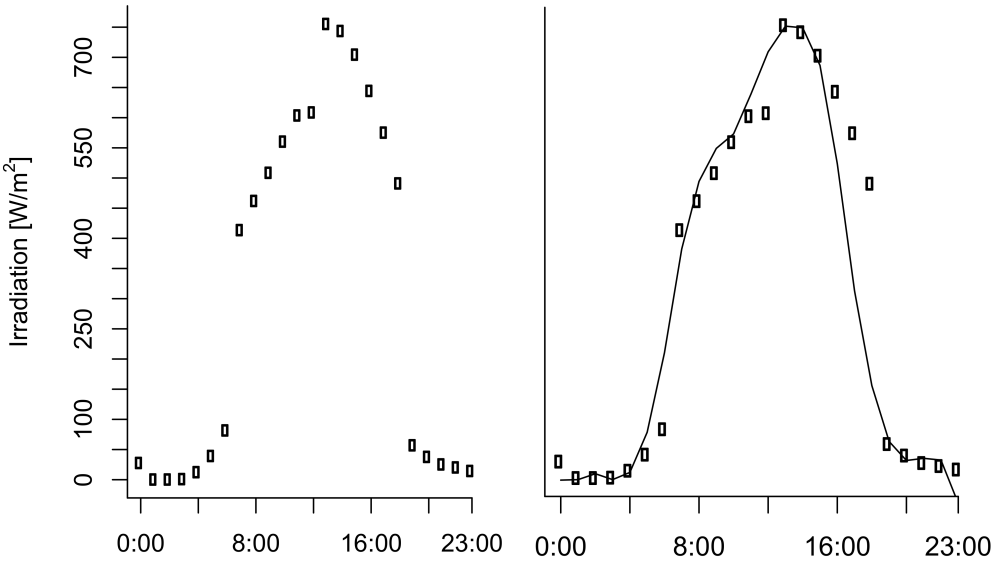

Figure 3. Solar irradiation 6-hour horizon forecasts (left) for the 21st of June 2017 (updated at 2 a.m., 8 a.m., 2 p.m. and 8 p.m.). Model of the real-time irradiation derived from a kernel smoothing approach on the updated forecasts (right).

3. Model

The model is a state-space model, derived from thermodynamic state equations describing the heat dynamics in the building as a lumped dynamic process model [25]. The model parameters are defined based on the building composition and structure. However, if the correct measurement data is available the model parameters could be estimated as in Reference [26], thus it would be easy to use the applied control setup in existing buildings, without the need for information about the building composition.

3.1. Assumptions

It is assumed that the building is just one big room with a flat roof. Thereto the following assumptions have been made; one uniform air temperature; no ventilation; no influence from the humidity of the air; no influence from the wind. The heat pump is assumed to be static because its dynamics are much faster than those of the building. Heat pumps require power to move heat from a cold space to a hot space using a refrigerant (it extracts heat from a cold space through an evaporator and delivers that heat to the hot space through a condenser). The heat pump efficiency is described using the COP-factor (Coefficient Of Performance). The maximum efficiency is modelled as the Carnot Efficiency [27] by

$$\mathrm{COP}_{\mathrm{Carnot}} = \left(1 - \frac{T_{\mathrm{cold}}}{T_{\mathrm{hot}}}\right)^{-1}, \tag{1}$$

where T_{hot} represents the condensation temperature, which is the temperature of the water flowing in the heating system (fluctuating in reality, but simplified to a constant = 40 °C). T_{cold} is the ambient evaporation temperature. However, the COP-factor is smaller in reality and therefore it is multiplied by another efficiency η, which can be assumed to be between 50% and 70% [28]. To be conservative, it has been set to 50% in the calculations. Therefore, the COP factor is expressed as

$$f_{\mathrm{cop}}(T_{\mathrm{hot}}, T_{\mathrm{cold}}) = \eta \cdot \mathrm{COP}_{\mathrm{Carnot}}. \tag{2}$$

3.2. State Space Equations

The state-space model is defined by dividing the building into three sections; '*Floor*', '*Interior*', and '*Inner envelope*'. *Inner* refers to the part of the walls and roof that is on the inside of the insulation.

The goal is to determine the temperature dynamics in the three sections. Thermodynamics can very well be explained in the same way as electric circuits, which will provide a nice analytic approach. The model is shown as the commonly used RC-diagram [24], in Figure 4.

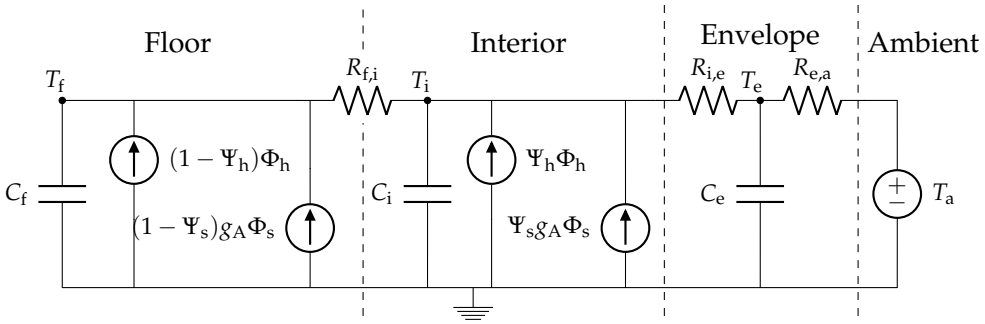

Figure 4. RC -network diagram of the model (floor heating).

$$\frac{\mathrm{d}T_t^f}{\mathrm{dt}} = \frac{1}{C_{\mathrm{f}}}\left(\frac{T_t^i - T_t^f}{R_{\mathrm{f,i}}} + (1-\Psi_s)g_{\mathrm{A}}\Phi_t^s + (1-\Psi_h)\Phi_t^h\right) \tag{3}$$

$$\frac{\mathrm{d}T_t^i}{\mathrm{dt}} = \frac{1}{C_{\mathrm{i}}}\left(\frac{T_t^f - T_t^i}{R_{\mathrm{f,i}}} + \frac{T_t^w - T_t^i}{R_{\mathrm{i,e}}} + \Psi_s g_{\mathrm{A}}\Phi_t^s + \Phi_t^h\Psi_h\right) \tag{4}$$

$$\frac{\mathrm{d}T_t^w}{\mathrm{dt}} = \frac{1}{C_{\mathrm{e}}}\left(\frac{T_t^i - T_t^w}{R_{\mathrm{i,e}}} + \frac{T_a - T_t^w}{R_{\mathrm{e,a}}}\right) \tag{5}$$

Refer to the nomenclature in Section 1 for variable definitions. Ψ_h is a logic variable integer (0,1) defining the heat system ($\Psi = 1$ for radiators and $\Psi = 0$ for floor heating). The heat delivered to the respective zones from the heat pump is

$$\Phi_t^h = f_{\mathrm{cop}}(40, T_t^a) \cdot P_t^e, \tag{6}$$

where P_t^e is the electrical power used by the heat pump. The solar irradiation P_t^s is going through the windows and heating both the floor and the room. Ψ_s describes the fraction that heats the room.

3.3. MPC

The model is transformed from continuous into discrete-time, see Reference [24]. The discrete-time linear state space model is written as

$$\boldsymbol{x}_t = \boldsymbol{A}\boldsymbol{x}_{t-1} + \boldsymbol{B}u_{t-1} + \boldsymbol{E}\mathbf{d}_{t-1} \tag{7}$$

$$y = \boldsymbol{C}\boldsymbol{x}_{t-1} + \epsilon_{t-1}, \tag{8}$$

where $\boldsymbol{x}$ is the state vector (building temperatures) and u is the controllable input vector describing is the electrical power to the heat pump, since the heat output from the heat pump, Φ_h, is a function of both the power input signal and the COP factor. $\mathbf{d}$ is the disturbances, which in this case is the outdoor temperature and solar irradiation. y_t is thus the controllable variable T_t^i plus some error ϵ_t. Hence

$$\boldsymbol{x}_t = \begin{bmatrix} T_t^i \\ T_t^f \\ T_t^w \end{bmatrix} \quad u_t = \begin{bmatrix} P_t^e \end{bmatrix} \quad \boldsymbol{d}_t = \begin{bmatrix} T_t^a \\ G_t \end{bmatrix}. \tag{9}$$

The matrix **A** states the dynamic behavior of the system, whereas matrix **B** specifies how the controllable input signals enter the system, and **E** specifies the uncontrollable input signals. Furthermore, $\boldsymbol{C}$ is a constant matrix that specifies the controllable state(s), in this case, $\boldsymbol{C} = \begin{bmatrix} 1 & 0 & 0 \end{bmatrix}$. For a deeper explanation, please refer to References [6] and [24].

The MPC then becomes a linear programming problem formulated as

$$\begin{aligned} \underset{u_s, v_k}{\arg\min} \quad & \sum_{k=1}^{N} \lambda_{t+k} u_{t+k} + p_k v_{t+k} \\ \text{subject to} \quad & \boldsymbol{X}_{s+1} = \boldsymbol{A}\boldsymbol{X}_s + \boldsymbol{B}\boldsymbol{u}_s + \boldsymbol{E}\boldsymbol{D}_s \\ & T_\mathrm{min} \leq \boldsymbol{C}\boldsymbol{X}_{s+1} + v_{s+1} \\ & T_\mathrm{max} \geq \boldsymbol{C}\boldsymbol{X}_{s+1} - v_{s+1} \\ & 0 \leq u_s \leq P_\mathrm{max} \\ & v_s \geq 0 \\ & \forall s \in \{t, t+1, t+2, ..., t+N\} \end{aligned}, \tag{10}$$

where λ_{t+k} is the penalty at time $t+k$, which in this case is the marginal CO_2 emission intensity. N is the prediction horizon. At each sampling time, the linear program is solved to obtain the heating schedule $[u_{t+1}, u_{t+2}, ..., u_{t+N}]$. $\mathrm{P_{max}}$ is the maximum power input signal the heat pump can receive. As it may not always be possible to meet the temperature demand, a slack variable v_k is introduced and connected to the violation penalty p_v. This value is set relatively high to avoid temperature violations.

This linear program is solved using lpsolve interfaced with the R-package *lpSolve*, [29].

4. Inputs for the Model

In this section, the reference buildings and input data are presented.

The Danish building codes specify the building law requirements and contain detailed requirements for all construction work. This study evaluates the building codes from 1977 to 2018, denoted $\mathrm{BC_{year}}$. The minimum requirements for outer walls, roof, windows and doors are listed by year in Table 1.

Two different types of buildings are considered; a family house and an office building, they differ in size and minimum temperature time settings during a nightly setback. The night time setpoint is 18 °C for (11 p.m.:5 a.m.) and (6 p.m.:7 a.m.) respectively for the family house and office building. During the day, the set point is 20 °C . The specific model parameters for each building are listed in Table 2 for a default case complying with $\mathrm{BC_{2015:2018}}$.

For the sake of simplicity, the buildings are squares with one story. Typical building part constructions are used, illustrated in Appendix B. The thickness of the concrete layers will be varied in the analysis.

The construction material properties are listed in Table A1 in Appendix C, where also the building dimensions and model parameters are defined.

The windows are defined as equal sizes on each side of the house pointing in north, east, south and west respectively with a window-to-wall ratio of 0.11 (the proportion of the wall that is windows). The R-package *solaR* is used for solar radiation inclination angle calculations. Ψ_s is set to 0.1 as in Reference [6].

Dimensioning of the heat pump is based on the heat loss from the buildings, specified in Appendix C.

Table 1. Building code requirements to insulation properties by year. Windows requirements are speficied with both U-values, glazing (g) and the estimated net heat transfer through the window into the room, E_{ref} (follows; $E_{\text{ref}} = 194.4\, g - 90.36\, U$).

BC	Walls	Roof	Doors	Windows		
Year	$U\left[\frac{\text{W}}{\text{m}^2\text{K}}\right]$	$U\left[\frac{\text{W}}{\text{m}^2\text{K}}\right]$	$U\left[\frac{\text{W}}{\text{m}^2\text{K}}\right]$	$U\left[\frac{\text{W}}{\text{m}^2\text{K}}\right]$	$E_{ref}\left[\frac{\text{kWh}}{\text{m}^2}\right]$	$g[-]$
1977	1	0.45	3.6	3.6	-174.314 **	0.777 **
1979–1985	0.4	0.2	2	2.9	-117.378 **	0.744 **
1995–1998	0.4	0.2	2	2.3	-69.934 **	0.709 **
2008	0.4	0.2	2	2	-46.909 **	0.688 **
2010	0.3	0.2	2	1.8 **	-33	0.673 **
2015–2018	0.14 *	0.1 *	2	1.6 **	-17	0.654 **

* U-values from ROCKWOOL A/S [30] needed to comply with the building envelope requirements. For the considered buildings the given U-values in $\text{BC}_{1977:2010}$ are strict enough to comply with the respective envelope requirements.

** Estimated values: From 2010, the windows insulation properties are described by E_{ref}. An exponential relationship between U and the glazing (g) is found from key numbers of different window types to be; $U = 0.0205e^{6.6545g}$[31]. This essentially allows U and g to be calculated from E_{ref}.

Table 2. Building dimensions and model parameters for both buildings based on BC_{2018}—calculations are as specified in Appendix C.

		Family House	Office Building
A_f	m^2	156	1250
A_w	m^2	107	302
A_{doors}	m^2	4	13
A_{windows}	m^2	14	39
$R_{\text{e,a}}$	$\frac{\text{K}}{\text{kW}}$	10.398	2.379
$R_{\text{i,e}}$	$\frac{\text{K}}{\text{kW}}$	1.190	0.269
$R_{\text{f,i}}$	$\frac{\text{K}}{\text{kW}}$	1.442	0.180
C_{e}	$\frac{\text{kWh}}{\text{K}}$	7.508	39.527
C_{f}	$\frac{\text{kWh}}{\text{K}}$	3.198	25.623
C_{i}	$\frac{\text{kWh}}{\text{K}}$	0.876	6.944

* The window and door area is determined from a window-to-wall ratio of 0.11 and a door-to-wall ratio of 0.04.

Forecasts

24 h horizon CO_2 emission forecasts presented in the related paper, [18], are used. The real-time values are presented in Section 2 along with estimated real-time values of the temperature and solar radiation. The weather forecasts have horizons of 24 h too.

To evaluate the MPC and the impact of using forecasts, different extreme cases are defined:

- **Case$_{\text{Ideal}}$**: This takes the exact value of a future CO_2 emission intensity as prediction hence, a perfect forecast. This provides an upper limit of CO_2 savings.
- **Case$_{\text{Real}}$**: This takes the CO_2 emission forecast developed in Reference [18] and represents the performance of the MPC with real forecasts.
- **Case$_{\text{Trivial}}$**: This makes no use of forecasts and will thus result in a non predictive controller that simply controls the heat pump keeping the temperature at the lower limit if possible.

5. Results and Discussion

In this section, various conditions and parameters are evaluated, for example, effect of horizon length, heat pump size, insulation and concrete thicknesses. The radiator and floor heating system is compared throughout the analysis along with the family house versus the office building. The criteria to be optimized is the CO_2 emission savings. The total emissions are calculated from: $\Lambda(\text{Case}) = \sum_{t=1}^{n-N} u_{\text{Case},t}\lambda_t$, where n is the number of data points presented in Section 2 ($n = 8688$) and the 'Case' denotes one of the three cases defined in Section 4. The savings are thus calculated as the flexibility index [32] by

$$Savings(Case) = \frac{\Lambda(\text{Case}_{\text{Trivial}}) - \Lambda(\text{Case})}{\Lambda(\text{Case}_{\text{Trivial}})} \tag{11}$$

As previously noted, this measure indicates the relative savings from utilizing the energy flexibility, hence not the absolute savings. If not otherwise stated the results are calculated with a building complying with BC_{2018}, see Table 1.

The parameters that will be investigated are:

- **Heating system and varying set points:** Both radiator and floor heating are considered and the use of varying set points (lower temperature during the night).
- **Horizon of forecasts:** To get an idea about how long horizons actually are needed to get a well performing MPC.
- **Size of heat pumps:** Essential for comparing the buildings and to know whether the potential is reached. Also economically, this is important because as the price increases with larger heat pumps. This will become a compromise between price and CO_2 emission. The default values for the family house and office are the minimum sizes required to meet the heat demand on the coldest day (-12 °C); 3 and 13 kW_{heat} respectively Appendix (see C for calculations). Requirements are thus a 1 and 4.3 kW input signal respectively according to Equation (1).
- **Insulation and concrete thicknesses:** These will be adjusted to see the impact of levels of insulation and heat capacity. The default thicknesses and material properties are shown in Appendix C.

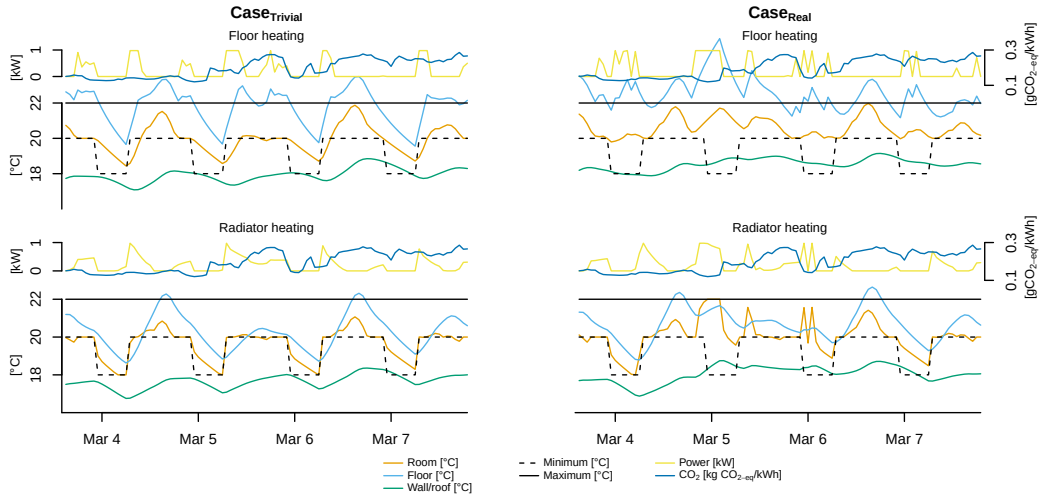

Figure 5. Varying temperature constraints–night [11pm:5am]; 18 °C . Note the CO_2 emission intensity and heating does not follow the Y-axis range, but rather the specified range in the colour legend.

An example of the differences between the cases, and the radiator and floor heating, is illustrated in Figure 5. The resulting electrical power and temperature for $\text{Case}_{\text{Trivial}}$ and $\text{Case}_{\text{Real}}$ on a four day period for the family house is shown. The result of $\text{Case}_{\text{Trivial}}$ is slightly different for the two heating systems. With radiators, it needs to heat more continuously than the floor heating throughout the day. This is because the radiators transfer the heat directly to the internal air, and not through the large heat capacity in the floor, resulting in a much faster response . In both cases, the heating is switched off during the night time to reach the lower set point. However, the floor heating violates the temperature restrictions more during the morning while heating the house, which is due to its slow response. $\text{Case}_{\text{Real}}$ seeks to only switch on the heat pump during low emission periods. The radiator system

does this well, but it is clearly limited by the maximum indoor temperature limit and the power input decays immediately to avoid temperature violation. In the floor heating system, the heat pump can operate at full load for a longer time using the floor as storage. An interesting point is that using day and night profiles, $\text{Case}_{\text{Real}}$ has no benefits of letting the temperature drop during the night because of: i) the temperature response is too slow and ii) the emissions are usually lowest during the night, so this is the best time to use the heat pump. Contrarily, the indoor temperature in the radiator system occasionally drops during the night if there is no significant drop in CO_2 emissions.

As expected, throughout almost a year ($n = 8688$ h) the floor heating system provides slightly more flexibility and reaches savings of 11% against 9% using radiators for the whole year for $\text{Case}_{\text{Real}}$.

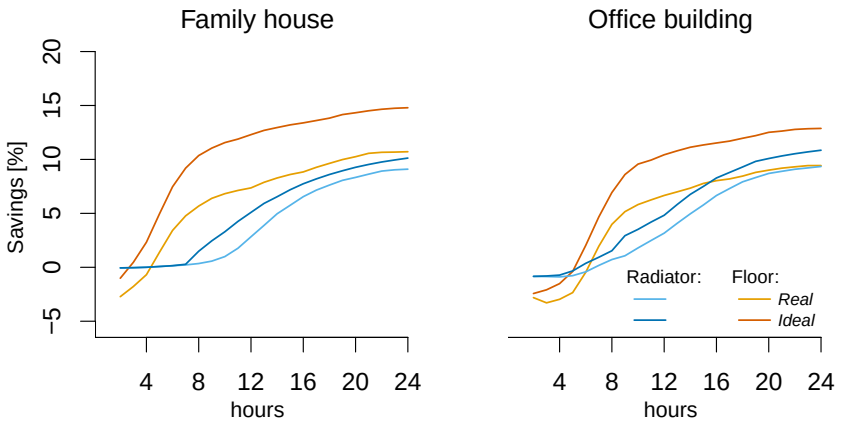

Figure 6. Savings with respect to the forecast horizon. Shown for both an ideal (perfect) and the Real forecasts.

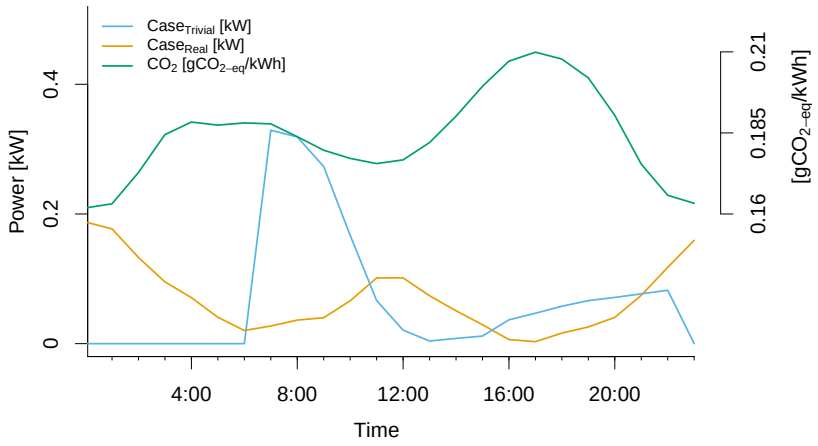

Figure 7. Average heat pump load in a family house with floor heating (200 mm floor concrete) versus the hour of the day for both $\text{Case}_{\text{Triviall}}$ and $\text{Case}_{\text{Real}}$. Hourly average marginal CO_2 emissions are shown in green.

The control horizon needs to be sufficiently long for the MPC to provide flexibility to the system (Figure 6). Note, the savings from floor heating become negative when using low control horizons. The nightly setback causes that; $\text{Case}_{\text{Trivial}}$ switches on at six AM every morning and the emission peak is happening already at four AM (Figure 7). For example, when using a two-hour control horizon, the heat pump will be forced to switch on at four AM instead and thus increase the emissions.

Interesting to note is the changing behaviour of the curves around the eight hours horizon: Case_{Ideal} in the family house with radiators has no savings up until this point. Like any other energy storage, a loss is introduced, in this case, by an increase in temperature resulting in a higher heat loss. Therefore, the MPC will only store heat if the CO_2 variations are large enough for the resulting emissions to break even with

the increased losses. These variations become sufficiently large around eight hours. This is less of a problem for the floor heating system, as the loss is much lower. This behaviour is less pronounced in the office building with radiators because the volume to surface area increases with larger buildings, hence the heat capacity increases relative to the surface area.

The loss in savings due to forecast errors, can be found from the difference between *Ideal* and *Real*. The radiator system is close to reaching its full potential, where the floor heating still can improve maximum about 5% savings from better forecasts.

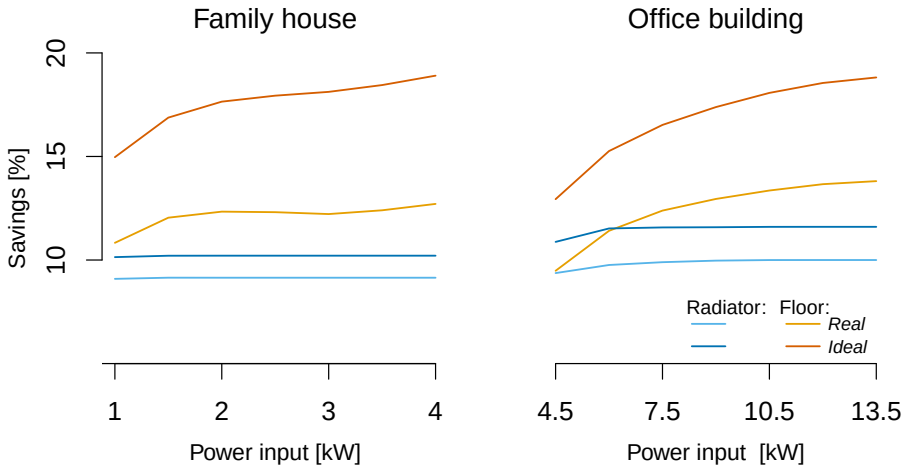

Figure 8. CO_2 emission reduction as a function of the size of the heat pump in kW shown for the real forecasts.

Finally, it is noted, that there is still an increase in savings at the 24 h horizon, for all scenarios, indicating that even longer horizons will lead to further increase in savings.

Increasing the heat pump size can lead to slightly higher savings (Figure 8), as more heat can be produced around the small-time slots with low emission. This is especially true when using floor heating, due to the high heat capacity in the floor. For the radiator systems, there is no significant gain for either the family house nor the office building. For the family house with floor heating, there is a relatively large gain when considering Case_{Ideal}, while Case_{Real} only reaches a slight improvement. There are significantly higher savings to achieve from Case_{Real} in the office building; because of the larger floor to wall area ratio (more heat capacity relative to the area the heat can escape through), a larger heat pump can accumulate more heat and thereby increase the flexibility.

The impact from insulation is evaluated with respect to the development of building codes from 1977 and forward, which has been an increase in insulation, window and door requirements (see Table 1 for building code specs and corresponding physical values). Another important aspect is the concrete thickness in the floor because it increases the heat capacity and thus the heat storage capabilities. Generally, BC_{1977} houses have very minimal because of the low insulation restrictions—significantly improved in BC_{1979} (Figure 9 and Table 3). However, the office building using floor heating can provide savings of around 9% with 200 mm of floor concrete and following BC_{1977} restrictions. This is due to the floor to wall ratio—the larger it is, the more the concrete thickness in the floor can contribute, and the less the insulation in the walls contributes.

For radiator heating, the concrete thickness in the floor is not very important for the savings. Still, adding 50–80 mm can increase the savings by around 2.5–4% (Table 3), but any thicker layer will not increase the savings at all (i.e., the red colored area in the graphs for radiator heating can hardly be seen— Figure 9). The insulation thickness in the office building using radiators seems saturated after BC_{1979}. This may seem counter-intuitive, but in reality, with high thermal resistance, the model becomes more rigid and therefore, less flexibility is allowed to occur. Of course, the absolute CO_2 emission savings will increase with more insulation.

Floor heating in a thick concrete floor provides the most flexibility in both buildings (around 16–17% in both with 200 mm concrete and $BC_{2015:2018}$). This setup exploits the full potential of the large heat storage in the floor, but lacks to exploit the nightly decrease in set point, because of the slow temperature response. With only 10 mm of concrete, the savings are almost identical for radiator and floor heating (about 6% with $BC_{2015:2018}$ in all cases). Note that a concrete thickness of 10 mm is not common practise.

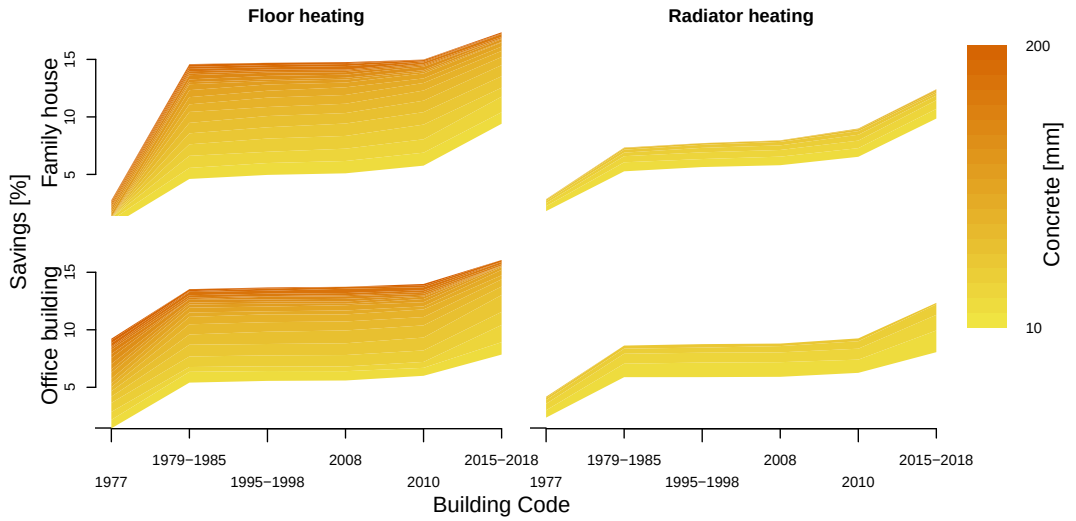

Figure 9. Savings with respect to the building code year and concrete thickness in the floor. Refer to Table 1.

Table 3. Min. savings are derived from a concrete thickness of 10 mm. Max. savings are derived from concrete thicknesses of 200 mm by default.

	Floor		Radiator	
	BC_{1977}	$BC_{2015:2018}$	BC_{1977}	$BC_{2015:2018}$
Family house				
Min. savings	0.5%	9.4%	1.8%	9.9%
Max. savings	2.7%	17.4%	2.8%	12.4%
Office building				
Min. savings	1.4%	7.8%	2.4%	8.1%
Max. savings	9.2%	16.0%	4.1%	12.3%

* Optimal concrete thickness of 50 mm. ** Optimal concrete thickness of 80 mm.

This study only measured the relative savings, but the absolute savings will, of course, also increase with more insulation. Therefore, if a house is not well insulated, the first attempt to decrease CO_2 emissions should be to reduce the heat demand by adding insulation before trying to optimize the control. As a result of new regulations in BC_{1979}, buildings in Denmark built before 1979 have been increasingly re-insulated to decrease the heat demand and costs. In Reference [33], it is found that the actual heat demand is on average lower than the theoretical calculations based on registered building data. This could imply that buildings indeed are re-insulated without further registration.

Most buildings in Denmark are built before 1979 [4], and this group is therefore the best representative for the potential buildings—floor heating is rarely the main heating system in this group. It would thus follow the early end of the radiator curves in Figure 9 with re-insulated buildings likely to comply with BC_{1979}. Therefore, between 4% and 7% of savings can be expected. However, new buildings complying with $BC_{2015-2018}$ envelope requirements and floor heating installed may reach savings of nearly 17%. Often, buildings combine radiators and floor heating and rely not only on one or the other, thus in reality have the advantages from both systems can be utilized depending on the heated rooms. Recall from Figure 5, the radiators are good at quick responses and therefore allows the temperature to decrease during the night contrarily to the floor heating. However, it has little capability of storing heat for more extended periods. The potential for this is open to further studies.

The average daily load for a $BC_{2015-2018}$ family house has shifted significantly (Figure 7). The trivial control follows to a certain degree the emissions throughout a day. The natural need for heating is therefore very inconvenient for the emissions and illustrates why energy flexibility is important. The MPC smooths the load during the day, decreasing it at otherwise peak hours and shifts most of the load to operate at midnight despite the lower temperature set point. This illustrates the importance of predictive control—if all houses follow the same schedule, there will be a need for much more additional storage capacity.

In general, this study can be relevant to buildings and scenarios with similar characteristic and climate conditions. Especially in the Nordic countries where the heating system comprises a large chunk of the electricity consumption. In warmer climates the study could be converted into air conditioning rather than heating. The wind and solar power production share was 36% in the examined region for the one year period in 2017 and 2018. The results will change depending on the conditions for example, with higher levels of fluctuating renewable generation in the future [34]. In a 100% renewable scenario it is of course not meaningful to use the CO_2 emissions as minimizing objective, however utilizing energy flexibility will be vital [35].

Model Simplification

The results are based on calculations using a simplified building model of a simplified building with only a single room. If more rooms are considered, it would add more heat capacity from walls dividing the rooms. This could increase the savings. Furthermore, a storage tank could have been added, which also could increase the savings as it would boost energy flexibility.

Disturbances, other than solar radiation and ambient temperatures, have been neglected in this study, for example, human activity. It is left as a point for future studies to include and assess the impact of building usage in the models and analysis.

6. Conclusions

The potential of achieving CO_2 savings using the energy flexibility of buildings has been analysed in a range of relevant scenarios including, both a family house and an office building. The simulated buildings were heated with heat pumps and the characteristics were varied according to the historical development of Danish building codes. The CO_2 level of the electricity generation for a year-long period in the Danish area DK2 was used as input, together with weather data from the area.

The results show considerable CO_2 savings for both radiator and floor heating systems. Forecast horizons should be 24 h or longer to obtain the full savings potential. Over-dimensioning the heat pump to increase flexibility turns out only to yield significant savings with floor heating, especially in the office building due to its larger storage area relative to the wall area.

Complying with $BC_{2015:2018}$ requirements, savings can reach around 17% using floor heating with 200 mm of floor concrete and 12% using radiators (Table 3). Generally, buildings must comply with building codes later than 1977 to achieve any considerable savings due to the low requirements in BC_{1977}.

Predictive control is vital to eliminate the peak hours, especially happening in the morning after the nightly setback, which is common practise. It is able to shift the demand to periods, where the coal power production is low, typically out of cooking peaks and during night time.

Author Contributions: conceptualization, R.G.J. and P.B.; methodology, K.L. and A.T.; software, R.G.J., K.L. and R.E.; validation, K.L.; formal analysis, K.L.; investigation, K.L.; resources, R.G.J., P.B. and H.M.; data curation, K.L. and O. Corradi; writing—original draft preparation, K.L.; writing—review and editing, R.G.J., P.B., O.C., R.E. and H.M.; visualization, K.L.; supervision, R.G.J. and P.B.; project administration, P.B., H.M.; funding acquisition, P.B., H.M. All authors have read and agreed to the published version of the manuscript.

Funding: This research was supported through the project "Smart Cities Accelerator 2016–2020" funded by the EU program Interreg Öresund-Kattegat-Skagerrak, the European Regional Development Fond and the CITIES project (DSF1305-00027B).

Acknowledgments: We are thankful for Tomorrow (www.tmrow.com) who has provided the data used in this study (including emission calculations for the bidding zone DK2).

Conflicts of Interest: The authors declare no conflict of interest. The funders had no role in the design of the study; in the collection, analyses, or interpretation of data; in the writing of the manuscript, or in the decision to publish the results.

Abbreviations

The following abbreviations are used in this manuscript:

MDPI	Multidisciplinary Digital Publishing Institute
CHP	Combined Heat and Power
MPC	Model Predictive Control

Appendix A. Kernel Smoothing

The 1 to 6 h horizon solar radiation forecasts are smoothed in order to remove large shifts in value, thus providing a better representation of real conditions.

Assuming horizons for $h = 1$ are the most accurate forecasts, a kernel smoothing process using a weight for short horizon favouritism is applied. The kernel weight, $\mathbf{w}_1$, is defined as the Epanechnikov kernel;

$$\mathbf{w}_1 = \frac{3}{4}(1 - \mathbf{u}^2), \tag{A1}$$

where $\mathbf{u} = \frac{|x_i - \mathbf{x}|}{b}$. $\mathbf{x}$ is a vector $[1, 2, .., n]$, where n is the number of data points and b is the bandwidth. The short horizon favoritism weight is defined as

$$\mathbf{w}_2 = \mathbf{e}^{-\frac{a}{\mathbf{h}-1}}, \tag{A2}$$

where $\mathbf{h} \in [1, 2, ..., 6]$ represents the hours in advance to the observation the forecast was received. Together, $\mathbf{w}_1$ and $\mathbf{w}_2$ define the final weight function; $\mathbf{w} = \mathbf{w}_1 \cdot \mathbf{w}_2$. This is applied into a linear regression model

$$\begin{gathered} \mathbf{y} = \mathbf{X}\boldsymbol{\beta} + \epsilon, \\ \text{for } \epsilon \sim N(0, \sigma^2 I), \end{gathered} \tag{A3}$$

where $\boldsymbol{X}$ is the input matrix (explanatory variables; hour, day and month), $\boldsymbol{y}$ is the output vector (response variable: Solar irradiation) and $\boldsymbol{\beta}$ is a vector of regression coefficients to be found. ϵ represents the normally distributed errors in the model.

The least square regression is performed to minimize

$$S(\boldsymbol{\beta}) = ||\mathbf{y} - \mathbf{X}\boldsymbol{\beta}||^2$$

and obtain the weighted least-squares solution

$$\boldsymbol{\beta} = (\mathbf{X}^T\mathbf{w}\mathbf{X})^{-1}\mathbf{X}^T\mathbf{w}\mathbf{y}. \tag{A4}$$

where $\mathbf{W}$ is the weight vector w. Using $a = 1.5$ and $b = 7$, the results are illustrated in Figure A1 (left plot). This is not sufficient on its own, as it does not manage to capture the curvature and midday peak. Therefore, the hour is converted into base splines (local polynomials between specified points called knots [36]);

$$bs(\mathbf{hour}_t) = \begin{bmatrix} bs_0(\mathbf{hour}_t) & bs_1(\mathbf{hour}_t) & \dots & bs_{df}(\mathbf{hour}_t) \end{bmatrix}^\top. \tag{A5}$$

where $\mathbf{hour}_t$ is the hour corresponding to the time step t. df is the degrees of freedom (essentially the number of splines; the higher the better it will fit the actual values). Using $df = 7$, the final result is illustrated in Figure A1 (right plot).

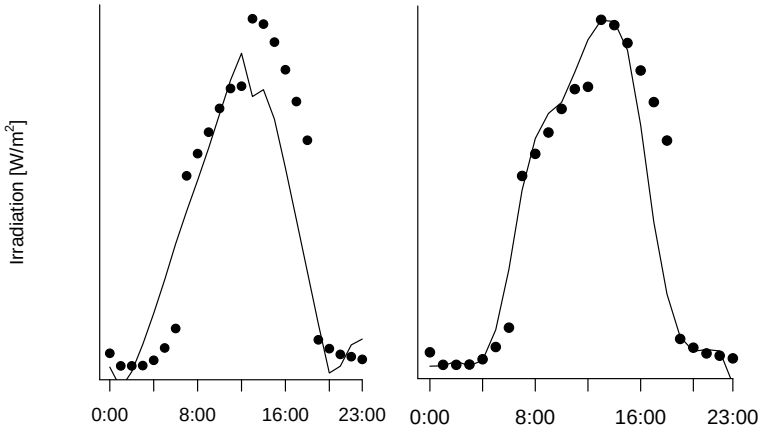

Figure A1. Solar irradiation 6 h horizon forecasts for the 21st of June 2017 (updated at 2 a.m., 8 a.m., 14 p.m. and 20 p.m.) and estimates of the real time irradiation (solid line) w/o splines (left). Estimates of the real-time irradiation using splines and the kernel smoothing approach (right)

Appendix B. Building Parts

The buildings consist of three parts; the walls, the floor and the ceiling. The material composition in each part is illustrated in Figure A2. Thereto, the model parameters (heat capacities and thermal resistances) are defined in Figure A3. The wall and roof are divided into the inner and outer part where only the inner temperature is modelled. The inner part is everything between the room and the insulation.

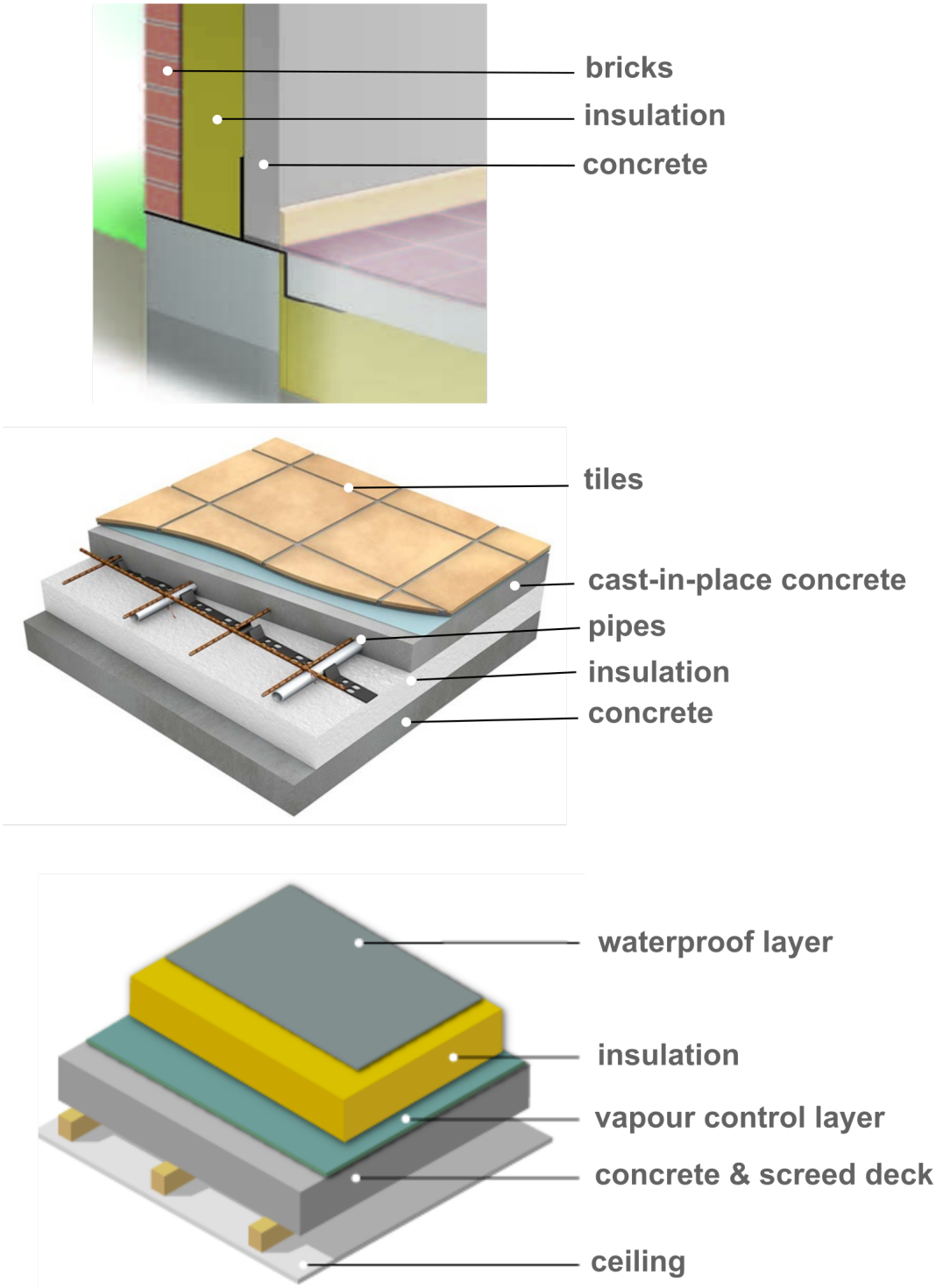

Figure A2. Typical constructions of walls (top), floor (middle) [37] and roof (bottom) [38].

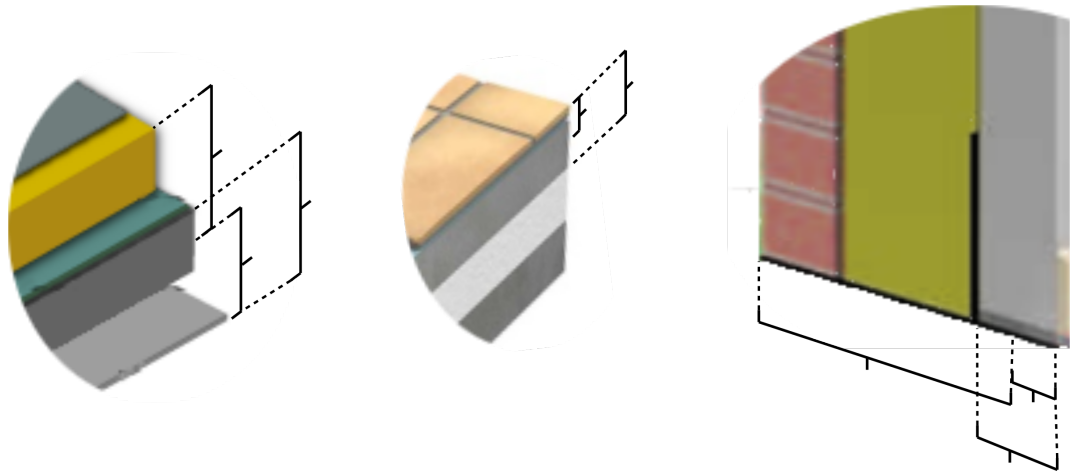

Figure A3. Definition of model parameters (heat capacities and thermal resistances) in the roof (left), floor (middle) and wall (right).

Appendix C. Parameter Estimation and Heat Pump Dimensions

The model parameters are defined illustratively in Figure A3. The materials used and corresponding properties are listed in Table A1.

Table A1. Thickness (ζ), density (ρ), heat capacity (C), thermal conductivity (k) and thermal resistance (R) of all the building parts. The thermal resistance is; $R = \frac{\zeta}{k}$. Thicknesses are examples for a BR18 building.

		Index	Material	ζ [m]	ρ [$\frac{kg}{m^3}$]	C[$\frac{J}{kg \cdot K}$]	k[$\frac{W}{m \cdot K}$]	R[$\frac{m^2 \cdot K}{W}$]
Wall	**Surface, outer**	w,s,o	-	-	-	-	-	0.06
	Outer	w,o	**Bricks**	0.15	1920	790	0.9	0.167
	Insulation	w,insul	**Rockwool**	0.12	240	710	0.042	2.693
	Inner	w,i	**Concrete, light weight**	0.10	1600	840	0.79	0.127
	Surface, inner	w,s,i	-	-	-	-	-	0.12
Roof	**Surface, outer**	r,s,o	**Waterproof layer**	0.01	0	0	0	0.06
	Insulation	r,insul	**Rockwool**	0.25	144	1000	0.058	4.304
	Air space	r,air	**Air**	0.05	1.225	1000	0.026	0.400
	Concrete	r,con	**Concrete, light weight**	0.05	1600	840	0.79	0.063
	Ceiling	r,cei	**Plaster light**	0.01	1680	840	0.81	0.012
	Inner surface	r,s,i	-	-	-	-	-	0.16
Floor	**Inner surface**	f,s,i	-	-	-	-	-	0.11
	Cover	f,cov	**Plywood**	0.01	545	1210	0.12	0.083
	Concrete	f,con	**Concrete, light medium**	0.05	1600	840	0.79	0.063
	Insulation	f,insul	**Rockwool**	0.30	240	710	0.042	7.143

Based on that, the parameters are calculated from Equation (A6) to (A15).

The thermal resistances, $R_{e,a}$, $R_{e,i}$ and $R_{f,i}$;

$$\boldsymbol{R}_{e,a} = \frac{1}{U_{windows} \cdot A_{windows} + U_{doors} \cdot A_{doors} + U_{w,a} \cdot A_w + U_{r,a} \cdot A_r} \tag{A6}$$

$$U_{w,a} = \frac{1}{R_{w,s,o} + R_{w,o} + R_{w,insul} + \frac{R_{w,i}}{2}} r \tag{A7}$$

$$U_{r,a} = \frac{1}{\frac{R_{r,con}}{2} + R_{r,insul} + R_{r,s,o}} \tag{A8}$$

$$\boldsymbol{R}_{e,i} = \frac{1}{U_{w,i} \cdot A_w + U_{r,i} \cdot A_r} \tag{A9}$$

$$U_{w,i} = \frac{1}{\frac{R_{w,i}}{2} + R_{w,s,i}} \tag{A10}$$

$$U_{r,i} = \frac{1}{\frac{R_{r,con}}{2} + R_{air} + R_{cei} + R_{r,s,i}} \tag{A11}$$

$$\boldsymbol{R}_{f,i} = \frac{1}{U_{f,i} \cdot A_f} \tag{A12}$$

$$U_{f,i} = \frac{1}{\frac{R_{f,con}}{2} + R_{cov} + R_{f,s,i}} \tag{A13}$$

As for the heat capacities; C_e is the sum of the heat capacity [kWh] in all the material on the inside of the insulation in the building envelope (concrete, air gap and ceiling). C_f is the sum of the heat capacity [kWh] in the floor concrete and tiles. C_i is estimated from a key number of 20 $\frac{kJ}{K \cdot m^2}$ [39], accounting for everything inside the room for example, air and furniture.

$$\boldsymbol{C}_e = \frac{1}{3.6E6}(\zeta_{w,i}\rho_{w,i}C_{w,i} \cdot A_w + (\zeta_{r,air}\rho_{r,air}C_{r,air} + \zeta_{r,con}\rho_{r,con}C_{r,con} + \zeta_{r,cei}\rho_{r,cei}C_{r,cei}) \cdot A_r) \tag{A14}$$

$$\boldsymbol{C}_f = \frac{A_f}{3.6E6}(\zeta_{f,cov}\rho_{f,cov}C_{f,cov} + \zeta_{f,con}\rho_{f,con}C_{f,con}) \tag{A15}$$

Heat Pump Dimensions

The minimum heat pump sizes are estimated from the heat loss on the coldest day. This is defined in Danish Standard DS-418 as an outdoor temperature of −12 °C with an indoor set point of 20 °C, thus $dT = 32$ °C.

$$Q_{loss} = (U_{walls} \cdot A_{walls} + U_{windows} \cdot A_{windows} + U_{doors} \cdot A_{doors} + U_{roof} \cdot A_{roof}) \cdot dT \tag{A16}$$

Note, the floor is neglected because the model assumes no heat loss through the floor. The heat losses are 2.9 kW and 13.4 kW for the family house and office building (danish building code of 2018) respectively. The maximum power input to the heat pump P_{max} is then $\frac{f_{cop}(40,-12)}{Q_{loss}}$, hence 1 kW and 4.5 kW.

References

1. Status of Power System Transformation 2019: Power system flexibility. 2019. In International Energy Agency. Avilable online: https://www.iea.org (accessed on 6 November 2019).
2. Huber, M.; Dimkova, D.;Hamacher, T. Integration of wind and solar power in Europe: Assessment of flexibility requirements. *Energy* **2003**, *69*, 236–246. [CrossRef]
3. Lund, H.; Mathiesen, B.V. Characterizing the energy flexibility of buildings and districts. *Appl. Energy* **2018**, *225*, 175–182. [CrossRef]
4. Bygninger og deres opvarmede areal efter område, tid, opvarmingsform, anvendelse, opførelsesår og enhed. 2019. By Danmarks Statistik. Available online: https://www.statistikbanken.dk/BOL102 (accessed on 27 November 2019).

5. *Danish Building Regulations 2018 (BR18)*; Ministry of Transport, Building and Housing: Copenhagen, Denmark, 2018. [CrossRef]
6. Halvgaard, R.; Kjølstad Poulsen, N.; Madsen, H.; Bagterp Jørgensen, J. Economic Model Predictive Control for Building Climate Control in a Smart Grid. In Proceedings of the 2012 IEEE PES Innovative Smart Grid Technologies (ISGT), Copenhagen, Denmark, 6–9 Ocotber 2012. [CrossRef]
7. Corradi, O.; Ochsenfeld, H.; Madsen, H.; Pinson, P. Controlling Electricity Consumption by Forecasting its Response to Varying Prices. *IEEE Trans. Power Syst.* **2013**, *28*. [CrossRef]
8. Clauß, J.; Stinner, S.; Solli, C.; Lindberg, K.B.; Madsen, H.; Georges, L. Evaluation Method for the Hourly Average CO2eq. Intensity of the Electricity Mix and Its Application to the Demand Response of Residential Heating. *Energies* **2019**, *12*. [CrossRef]
9. Oldewurtel, F.; Parisio, A.; Jones, C.N.; Gyalistras, D.; Gwerder, M.; Stauch, V.; Lehmann, B.; Morari, M.; Berkelaar, M.; Eikland, K.; et al. Use of model predictive control and weather forecasts for energy efficient building climate control. *Energy Build.* **2012** , *45* , 15–17, doi:10.1016/j.enbuild.2011.09.022. [CrossRef]
10. Oldewurtel, F.; Sturzenegger, D.; Morari, M. Importance of occupancy information for building climate control. *Appl. Energy* **2013**, *101*, 521–532. [CrossRef]
11. Killian, M.; Mayer, B.; Kozek, M. Cooperative fuzzy model predictive control for heating and cooling of buildings. *Energy Build.* **2016**, *112* , 130–140. [CrossRef]
12. Lindelöf, D.; Afshari, H.; Alisafaee, M.; Biswas, J.; Caban, M.; Mocellin, X.; Viaene, J. Field tests of an adaptive, model-predictive heating controller for residential buildings. *Energy Build.* **2016**, *99* , 292–302. [CrossRef]
13. Chen, C.; Wang, J.; Heo, Y.; Kishore, S. MPC-based appliance scheduling for residential building energy management controller. *IEEE Trans. Smart Grid* **2016**, *4* , 1401–1410. [CrossRef]
14. Chen, C.; Wang, J.; Heo, Y.; Kishore, S. Ten questions concerning model predictive control for energy efficient buildings. *Energy Build.* **2016**, *105* , 403–412, doi:10.1016/j.buildenv.2016.05.034.
15. Hammerstrom, D. *Pacific Northwest GridWise™ Testbed Demonstration Projects. Part I*; Pacific Northwest National Lab: Richland, WA, USA, 2007.
16. Wagner, U.; Mauch, W.; von Roon, S. *Das Merit-Order-Dilemma der Emissionen*; Forschungsstelle für Energiewirtschaft e.V.: Munich, Germany, 2002. [CrossRef]
17. Regettt A.; Böing F.; Conrad J.; Fattler S.; Kranner C.. Emission Assessment of Electricity: Mix vs. Marginal Power Plant Method. In Proceedings of the 15th International Conference on the European Energy Market (EEM), Lodz, Poland, 27–29 June 2018, doi:10.1109/EEM.2018.8469940.
18. Leerbeck, K.; Bacher, P.; Junker, R.; Goranović, G.; Corradi, O.; Ebrahimy, R.; Tveit, A.; Madsen, H. Short-Term Forecasting of CO_2 Emission Intensity in Power Grids by Machine Learning. *arXiv* **2020**, arXiv:2003.05740.
19. Corradi, O. Estimating the marginal carbon intensity of electricity with machine learning. 2018. in Medium. Available online: https://medium.com/ (accessed on 1 November 2019). [CrossRef]
20. Bialek, J. Tracing the flow of electricity. *Iee Proc. Gener. Transm. Distrib.* **1996,** *143* , 313–320.:19960461. [CrossRef]
21. Bialek, J. Contributions of Individual Generators to Loads and Flows . *Trans. Power Syst.* **1997**, *12*, 52–60, doi:10.1109/59.574923. [CrossRef]
22. Verhlst, C.; Logist, F.; Van Impe, J.; Helsen, L. Study of the optimal control problem formulation for modulating air-to-water heat pumps connected to a residential floor heating system. *Energy Build.* **2011**, *45*, 43–53, doi:10.1016/j.enbuild.2011.10.015.
23. Hangos, K.M.; Bokor, J.;Szederkényi, G. *Analysis and Control of Nonlinear Process Systems*. Springer: Berlin, Germany, 2003; pp. 39–71. [CrossRef]
24. Madsen, H.; Holst, J. Estimation of continuous-time models for the heat dynamics of a building. *Energy Build.* **1995**, *22*, 67–79, doi:10.1016/0378-7788(94)00904-X.
25. Madsen, H. *Time Series Analysis*; Chapman & Hall/CRC—Taylor & Francis Group: Boca Raton, FL, USA, 2007. [CrossRef]
26. Bacher, P.; Madsen, H. Identifying suitable models for the heat dynamics of buildings. *Energy Build.* **2011**, *43*, 1511–1522, doi:10.1016/j.enbuild.2011.02.005.
27. Cengel, Y.; Boles, M.A. *Thermodynamics—An Engineering Approach*; McGraw Hill: New York, NY, USA, 2010; pp. 82–84.

28. Coefficient of Performance. 2019. For De Kleijn Energy Consultants & Engineers. Available online: http://industrialheatpumps.nl/en/how_it_works/cop_heat_pump/ (accessed on 16 December 2019).
29. Berkelaar, M.; Eikland, K.; Notebaert, P. lpsolve: Open Source (Mixed-Integer) Linear Programming System. 2004. Available online: http://lpsolve.sourceforge.net/5.5/ (accessed on 2 May 2020).
30. *Den Lille Lune*; ROCKWOOL A/S: 2018; 34p. Availabel online: https://www.rockwool.dk/siteassets/o2-rockwool/dokumentation-og-certifikater/brochurer/bygningsisolering/den-lille-lune-rockwool.pdf (accessed on 2 May 2020). [CrossRef]
31. Viden Om Vinduer. 2020. By Energi Styrelsen. Available online: http://www.vinduesvidensystem.dk/ruder.html (accessed on 8 January 2020). [CrossRef]
32. Grønborg, R.; Armin, A.; Lopes, G.; Amaral, R.; Lindberg, K.B.; Reynders, G.; Relan, R.; Madsen, H. Characterizing the energy flexibility of buildings and districts. *Appl. Energy* **2018**, *225*, 175–182. [CrossRef]
33. Brøgger, M.; Bacher, P.; Madsen, H.; Wittchen, K.B. Estimating the influence of rebound effects on the energy-saving potential in building stocks. *Energy Build.* **2018**, *181*, 62–74, doi:10.1016/j.enbuild.2018.10.006.
34. *50% Wind Power in Denmark in 2025*; Ea Energy Analyses: Copenhagen, Denmark, 2007
35. Lund, H.; Mathiesen, B.V. Energy system analysis of 100% renewable energy systems—The case of Denmark in years 2030 and 2050. *Energy* **2009**, *34*, 524–531, doi:10.1016/j.energy.2008.04.003.
36. Hastie, T.; Tibshirani, R.; Friedman, J. *The Elements of Statistical Learning*; Springer Series in Statistics; Springer: Berlin, Germany, 2017; pp. 141–146.
37. Fix—rør i Monteringsbånd til Indstøbning. 2019. By Uponor. Available online: https://www.uponor.dk/vvs/produkter/gulvvarme/fix-gulvvarme-i-monteringsband (accessed on 1 November 2019).
38. Housing Retrofit: Concrete Flat Roof Insulation. 2019. By Greenspec. Available online: http://www.greenspec.co.uk/building-design/concrete-flat-roof-insulation/ (accessed on 1 November 2019).
39. *French Building Energy and Thermal Regulation*; CSTB FR: Marne-la-Vallee, France, 2005.